Electro-Thermo-Mechanical Simulation of AlGaN/GaN HEMTs

M. Auf der Maur, G. Romano and A. Di Carlo
Department of Electronic Engineering, University of Rome "Tor Vergata", 00133 Rome, Italy
Email: auf.der.maur@ing.uniroma2.it

Abstract— **A fully selfconsistent, coupled electro-thermo-mechanical model for nitride-based devices is presented and applied to a high-power AlGaN/GaN High Electron Mobility Transistor (HEMT). The influence of converse piezoelectric effect, thermal stress and of the selfconsistent coupling on the static device characteristics and on the stress distribution in the device is studied.**

INTRODUCTION

During the last years AlGaN/GaN High Electron Mobility Transistors (HEMTs) have been studied extensively for the use in high power microwave applications. The reliability of GaN-based HEMTs, however, still remains a major issue, which is usually assumed to be associated with strain- and temperature-related effects [1], [2], [3]. Simulation models including these effects are therefore of high interest for the understanding of device reliability.

Traditionally, simulation of GaN-based HEMTs has been based on the drift-diffusion or hydrodynamic model coupled to a thermal model, usually based on the Fourier model. Several coupled electro-mechanical simulation models for HEMTs have been proposed in the last years, too [4], [5]. A coupled electro-thermo-mechanical model has been reported in [6] and is based on a matlab-implemented strain calculation following a self-consistent thermoelectric TCAD simulation.

During the last year, increasing interest has been devoted to coupled electro-thermo-mechanical models [7], [8], [9]. In this work we present a fully selfconsistent, coupled electro-thermo-mechanical simulation model implemented in one single device simulation software [10].

G. Romano is now with the Department of Materials Science and Engineering, Massachusetts Institute of Technology

SIMULATION MODEL

Our simulation model is based on the self-consistent solution of the mutually coupled equations of the drift-diffusion/Poisson model for electronic transport (1)-(3), the Fourier model for heat transport (4) and the equations of linear elasticity (5) given by the set of conservation laws (using index notation and Einstein summing convention)

$$-\partial_i\left(\varepsilon_{ij}\partial_j\varphi - P_i\right) = e(p-n-C) \quad (1)$$
$$-\partial_i\left(\mu^n n\partial_j\phi_n + S^n\partial_j T\right) = -R \quad (2)$$
$$-\partial_i\left(\mu^p p\partial_j\phi_p + S^p\partial_j T\right) = R \quad (3)$$
$$-\partial_i\left(\kappa_{ij}\partial_j T\right) = H \quad (4)$$
$$-\partial_i\left(C_{ijkl}\partial_l u_k\right) = f_j\ , \quad (5)$$

where $\partial_i \equiv \partial/\partial_{x_i}$, ε_{ij} is the permittivity, P_i is the total electric polarization, e the elementary charge, and p, n and C are the hole, electron and net ionized doping or trap densities, respectively. μ^n and μ^p are the carrier mobilities, S^n and S^p the thermoelectric powers (Seebeck coefficients) for electrons and holes, respectively, and R is the net recombination rate. κ_{ij} is the total thermal conductivity, T the lattice temperature and H the total heat source originating from carrier transport [11]. C_{ijkl} is the elasticity tensor, u_k the displacement field and f_j a body force describing any source of mechanical stress. We assume small deformations such that strain can be written as $\epsilon_{ij} = \frac{1}{2}(\partial_j u_i + \partial_i u_j)$, and Hooke's law can be used to linearly connect stress to strain by $\sigma_{ij} = C_{ijkl}\epsilon_{kl}$.

The three models are mutually coupled as shown schematically in Fig. 1. The strain ϵ_{jk} obtained from the linear elasticity model induces a piezoelectric polarization field $P_i^{pz} = e_{i,jk}\epsilon_{jk}$ that enters the Poisson equation together with the spontaneous polarization, $e_{i,jk}$ being the piezoelectric tensor.

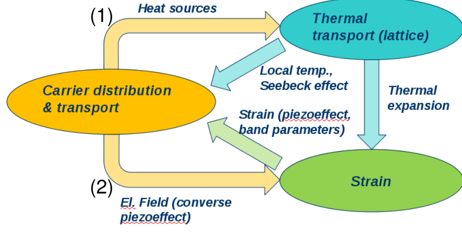

Fig. 1. The models and interactions involved in an electro-thermo-mechanical simulation.

The electric field E_i in turn induces a mechanical stress $\sigma_{jk} = e_{i,jk}E_i$ due to converse piezoelectric effect [12]. The transport model provides the heat source for the thermal model due to Joule and Thompson effect, whereas the temperature profile enters in the transport model by means of temperature dependent parameters and the Seebeck effect. The temperature profile also enters into the mechanical model due to the thermal expansion of the semiconductor lattice. This is modeled by introducing a thermally induced additional strain $\epsilon_{ij}^{th} = -\alpha_{ij}(T - T_0)$, where the α_{ij} are the thermal expansion coefficients and T_0 a reference temperature.

The lattice mismatch induced strain is treated following Ref. [13]. The total effective body force due to lattice mismatch, thermal stress and converse piezoelectric effect is then given by $f_j = -\partial_i \left\{e_{l,ij}E_l + C_{ijkl}\left[\epsilon_{kl}^0 - \alpha_{kl}(T - T_0)\right]\right\}$, where ϵ_{kl}^0 is the lattice matching strain.

The three models are solved iteratively for every operating point until appropriate convergence criteria are reached. The implementation is modular as shown in in Fig. 1, which allows single models to be substituted with different implementations.

Simulation Results and Discussion

We apply the model to an unpassivated $Al_{0.28}Ga_{0.72}N$/GaN HEMT with GaN cap layer (Fig. 2), comparing the results of selfconsistent electro-thermal (ET, neglecting coupling 2 in Fig. 1), electro-mechanical (EM, neglecting coupling 1 in Fig. 1) and fully selfconsistent electro-thermo-mechanical (ETM) simulations. For the thermal model we assumed an effective thermal resistivity of 8×10^{-8} m^2W/K such that the simulation reproduces reasonable peak temperatures. For the

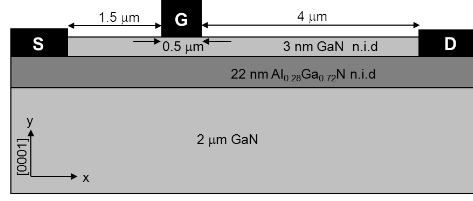

Fig. 2. The simulated $GaN/Al_{0.28}Ga_{0.72}N/GaN$ HEMT.

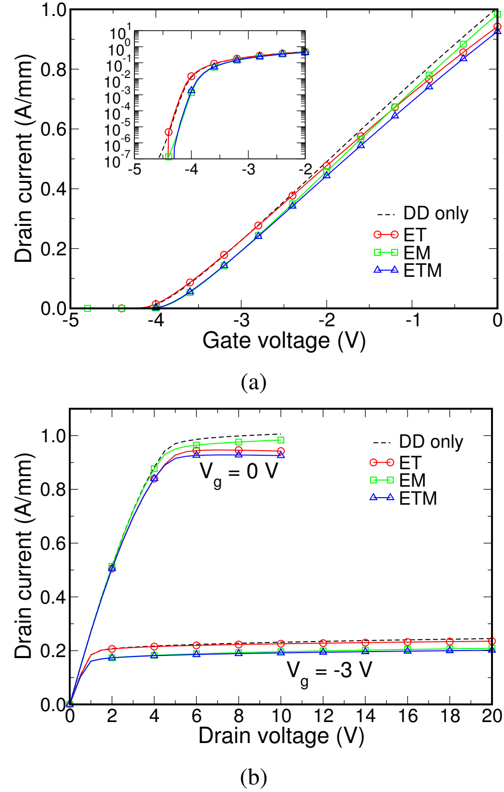

Fig. 3. Transfer (a, $V_d = 10$ V) and output (b) characteristics for the different model couplings. The dashed lines (DD) are results of a pure drift-diffusion simulation.

strain calculations we take as reference lattice the one of GaN at $T_0 = 300$ K, and for simplicity we keep this reference also under high power operating conditions. Elastic and piezoelectric constants are taken from [14].

Fig. 3 shows the transfer and output characteristics for the different model couplings. Apart from the well known thermal rollover, the strongest effect on electrical behaviour is due to converse piezoelectric effect, causing a slight positive shift of threshold voltage since the selfconsistent polarization field is smaller.

The selfconsistent temperature map for a power

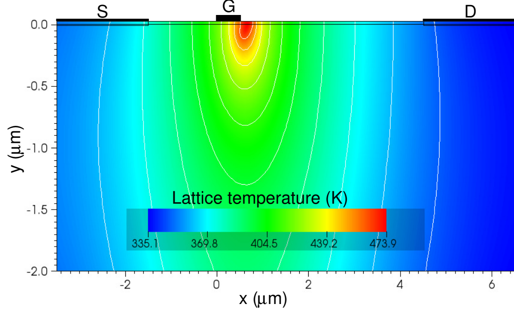

Fig. 4. Temperature map at V_d = 50 V, V_g = -3 V, P_{diss} = 11 W/mm.

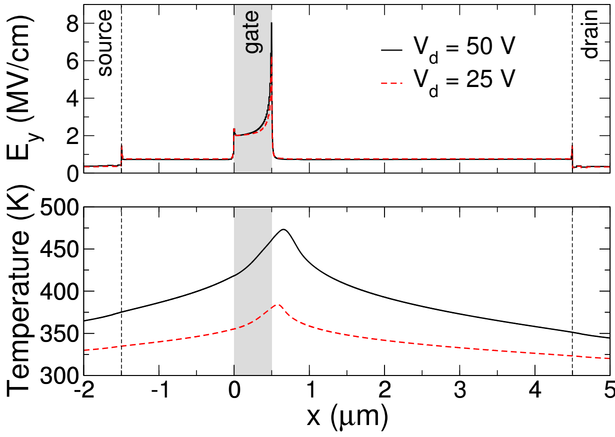

Fig. 5. Vertical electric field component E_y and lattice temperature along x-direction at the top end of the AlGaN barrier (ETM model).

dissipation of $\sim$ 11 W/mm can be seen in Fig. 4, showing a highly inhomogeneous temperature distribution in the device with the characteristic peak at the drain side of the gate.

Fig. 5 presents the vertical electric field E_x and the temperature along the x-direction at the top end of the AlGaN barrier, where electric field and strain are highest, for an operating point of V_d = 50 V, V_g = -3 V ($P_{\text{diss}} \sim$ 11 W/mm) and V_d = 25 V, V_g = -3 V ($P_{\text{diss}} \sim$ 5 W/mm), respectively, for the fully coupled ETM model. Due to the high peak electric field and the temperature peak and its gradient at the drain edge of the gate, the biggest impact of converse piezoelectric and thermal stress occur in the vicinity of the gate.

Fig. 6 shows planar stress and vertical strain components along the same cutline for the different model couplings for the 11 W/mm and 5 W/mm operating points. Converse piezoelectric effect leads to an increase of in-plane tensile stress and to a decrease of the compressive strain along growth direction. Thermal stress can be seen to have only minor effect on vertical strain, however it greatly reduces planar stress especially at high power levels, compensating therefore partially the influence of converse piezoelectric effect. This thermally induced reduction of mechanical stress has been observed experimentally [15] and is indeed compatible with the experimental finding that devices in on-state may suffer less or different type of degradation [16]. Moreover, whereas the converse piezoelectric stress is approximately isotropic in the xz-plane, thermal stress is highly unisotropic due to the different temperature gradients along x and z directions. Such unisotropic stress leads to resolved

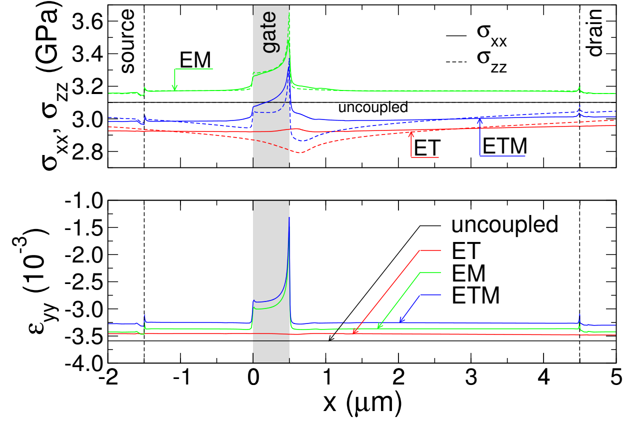

(a) P_{diss} = 11 W/mm

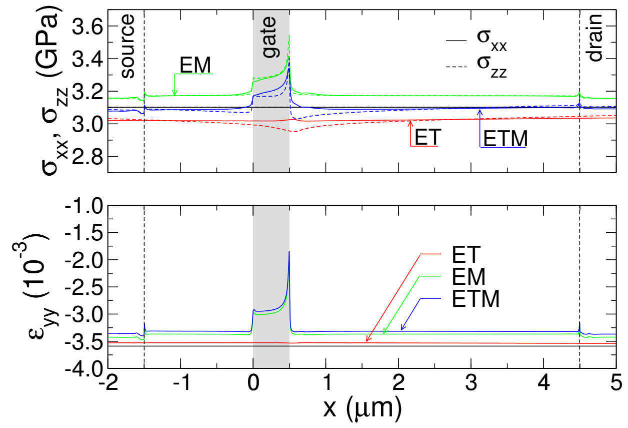

(b) P_{diss} = 5 W/mm

Fig. 6. Planar stress and vertical strain components at P_{diss} = 11 W/mm (a) P_{diss} = 5 W/mm (b), V_g = -3 V. Drain bias is 50 V and 25 V, respectively, for the ETM model and 43.5 V and 21.5 V, respectively, for the ET model.

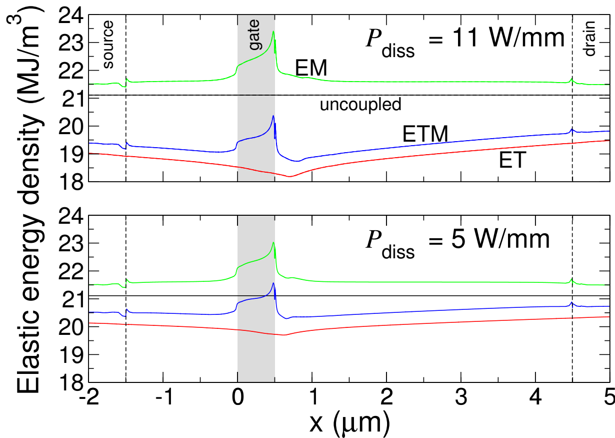

Fig. 7. Elastic energy density calculated as $\frac{1}{2}\epsilon_{ij}\sigma_{ij}$ for 11 W/mm (top) and 5 W/mm (bottom).

shear stresses of several 100 MPa on certain slip planes, which potentially could induce dislocation motion [17]. The principle stresses themselves seem to be too small to directly lead to mechanical failure, since yield strength in GaN is reported to be 10 – 15 GPa [18].

Fig. 7 shows the elastic energy at the top end of the AlGaN barrier along the x-direction. Thermal stress reduces the elastic energy density by a considerable amount at high power dissipation. This leads to lower planar elastic energy densities (obtained by integrating the elastic energy density along growth direction), decreasing the risk of arriving at critical values where inelastic strain relaxation by e.g. dislocation formation may set in [5].

References

[1] J. Joh and J. del Alamo, "Critical voltage for electrical degradation of gan high-electron mobility transistors," *Electron Device Letters, IEEE*, vol. 29, no. 4, pp. 287 –289, 2008.

[2] G. Meneghesso, G. Verzellesi, F. Danesin, F. Rampazzo, F. Zanon, A. Tazzoli, M. Meneghini, and E. Zanoni, "Reliability of gan high-electron-mobility transistors: State of the art and perspectives," *Device and Materials Reliability, IEEE Transactions on*, vol. 8, no. 2, pp. 332 –343, 2008.

[3] J. Wuerfl, E. Bahat-Treidel, E. Brunner, E. Cho, O. Hilt, P. Ivo, A. Knauer, P. Kurpas, R. Lossy, M. Schulz, S. Singwald, M. Weyers, and R. Zhynytska, "Reliability issues of gan based high voltage power devices," *Microelectronics Reliability*, vol. 51, p. 1710, 2011.

[4] B. Padmanabhan, A. Ashok, D. Vasileska, and S. Goodnick, "Modeling gan hemts using thermal particle-based device simulator," in *Semiconductor Device Research Symposium, 2009. ISDRS '09. International*, 2009, p. 1.

[5] J. Joh, F. Gao, T. Palacios, and J. A. del Alamo, "A model for the critical voltage for electrical degradation of gan high electron mobility transistors," *Microelectronics Reliability*, vol. 50, p. 767, 2010.

[6] F. Gao, H.-Y. Lo, R. Ram, and T. Palacios, "Self-consistent electro-thermal simulation of algan/gan hemts for reliability prediction," in *Device Research Conference (DRC), 2010*, 2010, p. 127.

[7] A. Prakash, R. Kumar, B. A. Prabowo, M. Kumar, Y. Shaoming, G. Sheu, and J.-R. Tsai, "Effects of SiO_2 passivation on AlGaN/GaN HEMT by self-consistent electro-thermal-mechanical simulation," in *10th Internationsla Conference on Electronic Measurement & Instruments*, 2011.

[8] M. G. Ancona, S. C. Binari, and D. J. Meyer, "Fully coupled thermoelectromechanical analysis of gan high electron mobility transistor degradation," *Journal of Applied Physics*, vol. 111, p. 074504, 2012.

[9] A. Venkatachalam, W. T. James, and S. Graham, "Electro-thermo-mechanical modeling of gan-based hfets and moshfets," *Semiconductor Science and Technology*, vol. 26, no. 8, p. 085027, 2011.

[10] TiberCAD simulation package, http://www.tibercad.org.

[11] G. K. Wachutka, "Rigorous Thermodynamic Treatment of Heat Generation and Conduction in Semiconductor Device Modeling," *IEEE Transactions on Computer-Aided Design*, vol. 11, pp. 1141–1149, Nov. 1990.

[12] L. C. Lew Yan Voon and M. Willatzen, "Electromechanical phenomena in semiconductor nanostructures," *J. Appl. Phys.*, vol. 109, no. 3, 2011.

[13] M. Povolotskyi and A. Di Carlo, "Elasticity theory of pseudomorphic heterostructures grown on substrates of arbitrary thickness," *J. Appl. Phys.*, vol. 100, p. 063514, 2006.

[14] O. Ambacher, J. Majewski, C. Miskys, A. Link, M. Hermann, M. Eickhoff, M. Stutzmann, F. Bernardini, V. Fiorentini, V. Tilak, B. Schaff, and L. F. Eastman, "Pyroelectric properties of Al(In)GaN/GaN hetero- and quantum well structures," *Journal of Physics: Condensed Matter*, vol. 14, no. 13, p. 3399, 2002.

[15] A. Sarua, T. Batten, H. Ji, M. J. Uren, T. Martin, and M. Kuball, "Thermal and Piezoelectric Stress in Operating AlGaN/GaN HFET Devices and Effect of the Fe Doping in the GaN Buffer Layer," in *CS MANTECH Conference*, 2009, p. 127.

[16] M. Faqir, G. Verzellesi, G. Meneghesso, E. Zanoni, and F. Fantini, "Investigation of high-electric-field degradation effects in algan/gan hemts," *Electron Devices, IEEE Transactions on*, vol. 55, no. 7, p. 1592, 2008.

[17] L. Sugiura, "Dislocation motion in GaN light-emitting devices and its effect on device lifetime," *J. Appl. Phys.*, vol. 81, no. 4, p. 1633, 1997.

[18] R. Nowak, M. Pessa, M. Suganuma, M. Leszczynski, I. Grzegory, S. Porowski, and F. Yoshida, "Elastic and plastic properties of GaN determined by nano-indentation of bulk crystal," *Applied Physics Letters*, vol. 75, no. 14, p. 2070, 1999.